

Analysis of Forbush decreases observed using a muon telescope in Antarctica starting on 21 June 2015^{*}

De-Hong Huang(黄德宏)^{1;1)} Hong-Qiao Hu(胡红桥)¹ Ji-Long Zhang(张吉龙)^{2;2)} Hong Lu(卢红)²
Da-Li Zhang(张大力)² Bin-Shen Xue(薛炳森)³ Jing-Tian Lu(吕景天)³

¹ SOA Key Laboratory for Polar Science, Polar Research Institute of China, Shanghai 200136, China

² Institute of High Energy Physics (IHEP), Chinese Academy of Sciences (CAS), Beijing 100049, China

³ Key Laboratory of Space Weather, National Center for Space Weather, China Meteorological Administration, Beijing 10081, China

Abstract: A cosmic-ray muon telescope has been collecting data since the end of 2014, which was shortly after the telescope was built in the Zhongshan Station of Antarctica. The telescope is the first observation device to be built by Chinese scientists in Antarctica. The pressure change is very strong in Zhongshan station. The count rate of the pressure correction results shows that the large variations in the count rate are likely caused by pressure fluctuations. During the period from 18 June to 22 June 2015, four halo coronal mass ejections (CMEs) were ejected from the Sun. These CMEs initiated a series of Forbush decreases (FD) when they reached the Earth. We conducted a comprehensive study of the intensity fluctuations of galactic cosmic rays recorded during FDs. The intensity fluctuations used in this study were collected by cosmic ray detectors of multiple stations (Zhongshan, McMurdo, South Polar, and Nagoya), and the solar wind measurements were collected by ACE and WIND. The profile of the FD of 22 June demonstrated a four-step decrease. The traditional one- or two-step FD classification method does not adequately explain the FD profile results. The interaction between the faster CME that occurred on 21 June 2015 and the two slow CMEs of the earlier few days should be considered. The cosmic ray intensities of the South Pole, McMurdo, and Zhongshan stations have similar hourly variations, whereas the galactic cosmic rays recorded between polar and non-polar locations are distinct. The FD pre-increase of 22 June 2015 for the Nagoya muon telescope (non-polar location) lags those of the McMurdo and Zhongshan stations (polar locations) by 1 h. The FD onset of 22 June 2015 for the Nagoya muon telescope lags those of the polar locations by 1 h.

Keywords: cosmic ray, muon telescope, neutron monitor, CME, Forbush decrease

PACS: 95.55.Vj, 96.40.Cd, 96.60.Wh **DOI:** 10.1088/1674-1137/42/12/125001

1 Introduction

The cosmic ray intensity decreased during the magnetic storm that occurred during April 25–30, 1937. This event was reported by Forbush [1], and it came to be referred to as the Forbush decrease (FD) in the 1950s. Hess and Demmelair confirmed the cosmic ray decrease phenomenon [2]. To explain the FD, Chapman assumed that the magnetic field of the equatorial ring-current protects the Earth from the approaching cosmic ray via shielding [3]. More detailed calculations showed that the influence of enhanced ring-current will lead to an increase in cosmic ray intensity, rather than to its decrease [4]. Using neutron monitors (NMs), Simpson showed that the FD is not produced by geomagnetic field variations [5]. Since the first years of the space era, FDs have been

recorded not only from the Earth but also from space. The galactic cosmic ray (GCR) intensity measurements collected from the Pioneer V spacecraft show that the FD was due to the Sun and was unrelated to the Earth and its magnetic field [6]. After PAMELA was launched in 2006, GCR spectra were measured directly with sufficient statistics to observe FDs [7].

Interplanetary coronal mass ejections (ICMEs), the interplanetary counterparts of coronal mass ejections (CMEs), are large magnetized clouds of plasma, ejected by the Sun and expelled into heliosphere. If the speed of the ICME exceeds that of the ambient solar wind by an amount greater than the fast magnetosonic wave speed, a shock wavefront and a magnetic sheath region are formed between the shock and the ICME leading edge. FDs caused by the ICMEs are sporadic (non-recurrent) and

Received 6 November 2017, Revised 25 August 2018, Published online 25 October 2018

^{*} Supported by NSFC (11575204)

1) E-mail: huangdehong@pric.org.cn

2) E-mail: zhangjl@ihep.ac.cn

©2018 Chinese Physical Society and the Institute of High Energy Physics of the Chinese Academy of Sciences and the Institute of Modern Physics of the Chinese Academy of Sciences and IOP Publishing Ltd

are characterized by fast decreases. FDs can drop to the minimum within approximately a day, but their gradual recovery phase can last several days. The magnitude of an FD, within the energy range of the NM, varies from a few percent to close to 30% (for example, the FD of 29 October 2003). Sanderson et al. (1991) have attempted to measure the effect of turbulence in the post shock region by measuring the radial diffusion coefficient from the magnetic field data, and relating this to the magnitude of the first-step FD [8]. Lockwood et al. observed that an FD is more likely to occur following a shock in which the magnetic field and plasma parameters are strongly enhanced. Their results indicate that a decrease in cosmic ray intensity may be produced by a smaller diffusion coefficient in the region behind the shock [9]. A simple model for propagating diffusive barriers was presented by Wibberenz et al. [10]. In this work, FDs can be interpreted in terms of radially propagating barriers with a reduced (radial) diffusion coefficient. Cane (2000) concluded that sporadic FDs can be divided into three types: FDs caused by only shocks, FDs caused by only ICMEs, and FDs caused by both shocks and ICMEs [11]. The traditional FD model predicts that an ICME and its shock reduce the GCR intensity via a two-step profile. After analyzing 233 ICMEs, which should have created two-step FDs, Jordan et al. concluded that small-scale interplanetary magnetic field (IMF) structures, which are generally ignored, can contribute to a variety of FD profiles [12].

An FD caused by corotating interacting regions (CIRs) formed by the interaction between a fast solar wind from a coronal hole and a slow solar wind can be recurrent. A recurrent FD has a long decrease phase. The average duration of the recurrent FDs is approximately 10–14 days. Generally, the decrease and recovery phases of the GCR intensity are symmetric [13].

An FD's profile may vary from one event to another because the interplanetary medium disturbance is a result of multiple factors. Cosmic-ray-based spectral variations and anisotropy associated with an FD provide valuable information to understand the interplanetary medium. Prior to the discovery of the solar winds and IMFs, only FDs were observed in the data. Consequently, valuable historical information was collected but not properly analyzed. Ground-based observations of cosmic rays are an important aspect of space weather prediction [14]. By using a cosmic-ray muon hodoscope, Munakata observed enhanced anisotropy prior to the arrival of interplanetary shocks during an FD [15].

The in situ measurements of cosmic rays using onboard satellite detectors are not affected by the atmosphere; however, satellite-based detectors always have very small detection windows and do not obtain sufficient statistics in the high-energy region. For instance,

the alpha magnetic spectrometer onboard ISS measures particles in the GV–TV rigidity range. Thus, it only provides high-energy solar energetic particles (SEPs) events at ~ 1 GV from 2011 to 2016 [16]. The major advantage of cosmic ray detectors on the ground is that the detection area is very large. Ground detectors (neutron monitor and muon telescope) can provide the intensity of cosmic rays from 500 MeV to 100 GeV with sufficient statistics. The geomagnetic cutoff rigidity of a detector determines the cosmic ray energy that reaches each observation station. Multiple space and ground observations are carried out simultaneously to provide complementary observations.

Since 1951, ground observations have been carried out via NMs around the world. The muon detectors complement NMs by monitoring cosmic ray modulations occurring at slightly higher energies and provide measurements of numerous muon arrival directions. The surface muon detectors can detect events with a median primary energy of 50–100 GeV, whereas NMs only detect energy of 10–40 GeV. Global muon detector networks (GMDNs) were established in March 2006 to monitor space environments. The networks include multidirectional detectors (36 m²) in Nagoya, Japan, a hodoscope-type cosmic ray detector (9 m²) in Kuwait, a muon detector (36 m²) in Sao Martinho, Brazil, and a muon detector (9 m²) in Hobart, Australia [17].

A new muon-neutron telescope was set up in Yangbajing in 2007 [18]. The Yangbajing Cosmic Ray Observatory is located at a latitude of 30.11°N, a longitude of 90.53°E, and an altitude of 4300 m above sea level. Using IGRF1995, the vertical cutoff rigidity of cosmic rays is determined to be 14.1 GV.

By the end of 2014, a cosmic-ray muon telescope was installed at Zhongshan Station in Antarctica [19]. It is located at sea level with a latitude of 69.4°S and a longitude of 76.4°E. Using IGRF1995, the vertical cutoff rigidity of cosmic-ray protons at Zhongshan Station is determined to be 0.07 GV. The observation data are sent to China via a satellite link released through a network. Every hour, the raw data of the muon telescope are transmitted from Zhongshan station to Institute of High Energy Physics (IHEP) in Beijing. The data are published on the Internet in real time [20].

Between 18 and 22 June 2015, four halo CMEs were ejected toward the Earth and initiated a series FDs. We examine the sequence of solar events that occurred during 18–22 June 2015 and how they affected the counting rates of the Zhongshan muon telescope. A comparative analysis of this series of FDs with those of Zhongshan, McMurdo, South Polar, and Nagoya was performed. This is the only time that a surface muon telescope recorded this series of FDs in Antarctica.

The rest of this paper is organized as follows. In Sec-

tion 2, we briefly describe the setting of the Zhongshan station muon telescope (ZSMT). The observed results of this series of FDs are discussed in Section 3. Finally, a summary is detailed in Section 4.

2 Zhongshan station muon telescope

By the end of 2014, a cosmic-ray muon telescope was installed at Zhongshan Station. First, we describe the setting of the ZSMT. The meteorological effects of the observational data of ZSMT are discussed later.

2.1 Setting

The ZSMT consists of two plastic scintillator detectors. Each scintillator is a $50\text{ cm} \times 50\text{ cm} \times 2\text{ cm}$ ($L \times W \times H$) rectanguloid. The light guide box of the detector is shaped like a pyramid and a layer of Tyvek reflective film is attached to the inner surface of the box to increase its light-collecting ability. The vertical spacing between the two scintillators is 75 cm. The two scintillators are used to determine the incidence direction of muons. A photomultiplier tube (PMT) is mounted above the scintillator at a vertical distance of 50 cm in order to achieve higher light-acceptance uniformity. When a cosmic-ray muon arrives and subsequently passes through the upper and lower detectors simultaneously, a coincidence pulse is produced. The numbers of coincidence pulses are recorded via a counter. Every second, the collected data are sent to the data acquisition computer. For the convenience of conveying and installing, the lead plate used for the absorption of the soft components of cosmic rays between the two scintillators was not installed.

2.2 Meteorological effects of ZSMT observational data

Figure 1 shows the hourly cosmic-ray and atmosphere pressure measurements observed by the ZSMT during 1–30 June 2015. The pressure change at Zhongshan station is very strong, fluctuating between 963.85 hPa and 1004.93 hPa with a maximum change value of approximately 41 hPa. Compared with Yangbajing station, the pressure change of Tibet fluctuated between 596.78 hPa and 607.48 hPa and had a maximum change value of approximately 10 hPa for the same period. In Fig. 1, the detector count rate has a strong anti-correlation with pressure. A pressure correction of the muon data (collected by the ZSMT) is likely required.

The pressure-corrected count formula is $N_{\text{cor}} = N_{\text{obs}}/e^{\beta(P-P_0)}$, where P_0 is the mean pressure. The observed data were collected between 1 May and 20 June, i.e., before the IMF distribution. The mean pressure for this period is 985.44 hPa and the mean hourly count is 33811. By adopting the method available in reference [21], the coefficient of pressure correction β is determined

to be -0.16% /hPa. The hourly pressure-corrected muon count collected in June is shown in Fig. 2. The mean hourly pressure-corrected muon count for the period between 1 May and 20 June is 33885. From a comparison between Figs. 1 and 2, the pressure-corrected counts are evidently different from the uncorrected counts. The counts in Fig. 2 do not have large peak and although variations similar to those observed in Fig. 1. In Fig. 2, the counts have a significant diurnal variation. In fact, most of the large variations in the count rate are likely caused by pressure fluctuations.

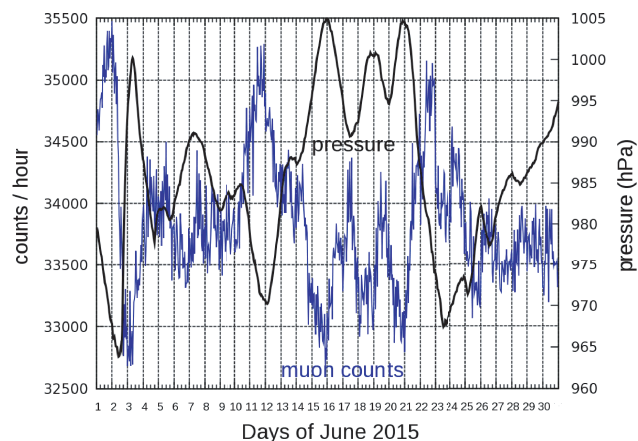


Fig. 1. (color online) Meteorological effect of ZSMT data from 1 to 30 June 2015

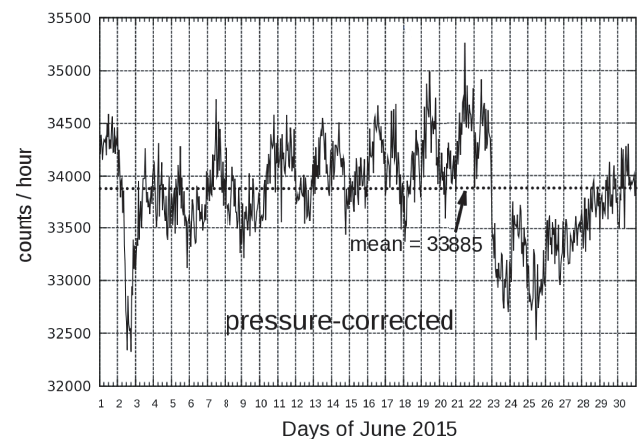


Fig. 2. Hourly pressure-corrected muon counts from 1 to 30 June 2015

Although the pressure-corrected counts show a significant diurnal change, there is a significant disturbance in the diurnal variation. Owing to the complexity of the atmospheric environment at Zhongshan station, other types of atmospheric correction should be investigated. Many detector-based counts depend on the surface temperature. The Zhongshan muon detectors are installed inside a building and the indoor temperature is maintained at approximately 26° . Muon detector counts often correct for temperature in the upper atmosphere.

The correction is not applied as no temperature data are available for these regional atmospheres. In general, such data should be available from satellite data collections. Corrections for temperature fluctuations in the upper atmosphere need to be considered in the future.

3 Observations of FDs starting on 21 June 2015

An impressive series of solar events that occurred in June 2015 were caused by the active region (AR) 12371. The Earth experienced a geomagnetic storm on 22 June 2015 owing to the arrival of an Earth-directed CME on 21 June 2015. Coronal material exploded from the sun with the velocity of 1366 km/s, arriving at Earth at 18:33 UT on 22 June 2015. The CME was associated with an M2.0 flare from N12°E13° peaking at 01:42 UT on 21 June 2015. The LASCO coronagraphs onboard the SOHO satellite first observed the halo CME at 02:36 UT [22]. The same active region produced two other CMEs in the earlier few days, which were pushed (or compressed) along by the faster Earth-directed CME that occurred on 21 June 2015. The sudden storm commencement (SSC) identified itself with the arrival of the ICME shock at 18:33 UT on 22 June 2015. This ICME was recorded from 02:00 UT on 23 June 2015 to 14:00 UT on 24 June 2015

[23]. A shock that overtook the ICME at 1 AU arrived at 13:29 UT on 24 June 2015. This shock is associated with an ICME from 10:00 UT on June 25 2015 to 06:00 UT on June 26 2015. This ICME is related to the halo CME released at 18:36 UT on 22 June 2015. Piersanti et al. have provided a comprehensive analysis of this series of CME events [24]. In addition to this analysis, further investigations of the GCR ground observations are required to explain this unique series of events and associated heliospheric configurations. During these fast ICMEs, which were directed toward the Earth, a series of FDs was recorded. We subsequently examine the sequence of solar events that occurred during 18–22 June 2015 and how they affected the counting rates of the ZSMT.

3.1 Solar wind measurements

During the period from 18 to 22 June 2015, four Halo CMEs were ejected from the Sun [25]. Solar wind parameters observed by the ACE and WIND for the period 21–24 June 2015 are shown in Fig. 3. The figure shows the magnetic field intensity B , magnetic field B_x , B_y , B_z (in the GSE coordinate system) component, solar wind proton density n_p , solar wind proton temperature T_p , solar wind proton speed V_p , and the geomagnetic activity index Dst.

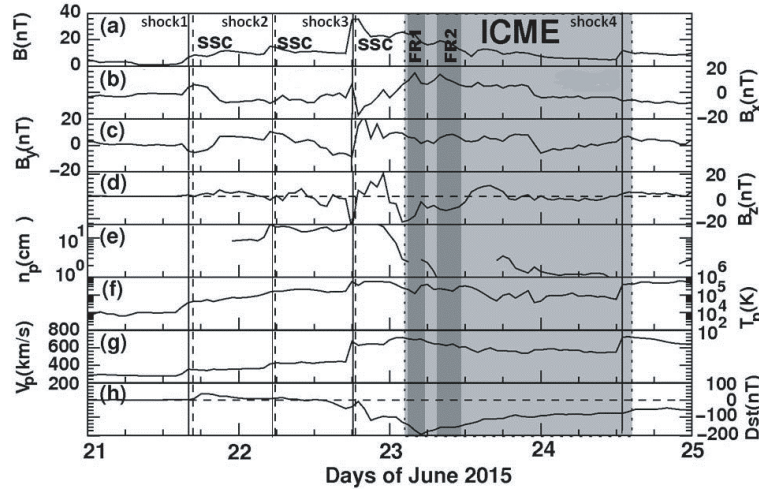


Fig. 3. Solar wind measurements from ACE and WIND. Data are plotted for the period 21–25 June 2015. The figure from top to bottom shows the hourly values of (a) the magnetic field strength B (nT) in the GSE coordinate system, (b) the magnetic field component B_x , (c) the magnetic field component B_y , (d) the magnetic field north–south component B_z , (e) the solar wind proton density n_p , (f) the solar wind proton temperature T_p , (g) the solar wind proton speed V_p , and (h) the geomagnetic activity index Dst. The times at which the shock crosses the WIND and SSC are shown using solid and dashed vertical lines, respectively. The shaded grey area indicates the interval of an ICME. Two small flux ropes, FR1 and FR2, are identified within the ICME.

Table 1. Selected CMEs and their corresponding shock/ICME

CME	shock	SSC	ICME start	ICME end
18 June 17:24	21 June 16:04	21 June 16:43		
19 June 06:42	22 June 05:02	22 June 05:45		
21 June 02:36	22 June 18:08	22 June 18:33	23 June 02:00	24 June 14:00
22 June 18:36	24 June 13:07	24 June 13:29	25 June 10:00	26 June 06:00

Four shocks passed through the WIND at 16:04 UT (shock1) on 21 June 2015, at 05:02 UT (shock2) on 22 June 2015, at 18:08 UT (shock3) on 22 June 2015, and at 13:07 UT (shock4) on 24 June 2015. The interplanetary shocks observed by the WIND can be found in the Yearly Summary of the CfA Interplanetary Shock Database [26]. The shock times are shown using a solid vertical line. The time of the ICME is associated with the geomagnetic SSC and is typically related to the arrival of a shock at the Earth. This information can be found in Service International des Indices Geomagnetique [27]. The start times of the SSC are shown using a dashed vertical line.

The ICME content from the list entitled “Near-Earth Interplanetary Coronal Mass Ejections since January 1996” was compiled by Ian Richardson and Hilary Cane [23]. The ICME collection started at 02:00 UT on 23 June 2015 and ended at 14:00 UT on 24 June 2015. The area shaded in gray indicates the interval of an ICME. As defined by Burlaga and co-workers, magnetic clouds are structures associated with a subset of ICMEs with enhanced (>10 nT) magnetic fields rotating smoothly through a large angle at low proton temperatures and low beta plasma [28, 29]. The ICME shows evidence of a rotation in the field direction but lacks some other characteristics of a magnetic cloud (e.g., enhanced magnetic field). The mean speed of this ICME is 610 km/s; this result is based on solar wind speed observations measured at the start and end times of the ICME. The maximum solar wind speed is 724 km/s during the period from the disturbance of the shock to the trailing edge of the ICME. By examining Fig. 3, we observe that the magnetic field component of this ICME shows large fluctuations without the smooth and regular shapes expected for a flux-rope topology [30]. Liu showed that two small flux ropes, FR1 and FR2, originated in the interaction of the ICME with the heliospheric current sheet [31].

In Section 3.3, the shocks and their corresponding CMEs, an application of the WSA-ENLIL model, were investigated. The first shock (shock1) was driven by the CME on 18 June 2015. The second shock (shock2) was associated with the CME on 19 June 2015. The ICME and its preceding shock (shock3) were produced by the CME on 21 June 2015. The fourth shock (shock4) was driven by the CME on 22 June 2015 and overtook the ICME at 1 AU. We list these events in Table 1. The first, second, and third columns indicate the date and time (UT) of the first appearance in the LASCO/C2

field-of-view, the shock arrival time at the WIND, and the associated SSC (typically related to the arrival of a shock on the Earth), respectively. The fourth and fifth columns are the ICME start and end times, respectively.

3.2 ZSMT observation

From 13 to 22 June 2015, four halo CMEs headed toward the Earth. Four shocks that accompanied these CMEs passed the WIND and produced a series of FDs. We examined the sequence of solar events that occurred during 18–22 June 2015 and how they affected the counting rates of the ZSMT between 21 and 30 June 2015.

As described in Section 2.3, the pressure change is very strong at Zhongshan station. A correction based on pressure is required to correct the muon data collected from the ZSMT. The hourly counts during the period 1 May to 20 June 2015, before the IMF distribution on 21 June 2015, were used to determine the hourly mean count, which is 33885. Fig. 4 shows the hourly plots of the magnetic field intensity B and B_z , the magnetic field turbulence level $\sigma(\%)$, the solar wind proton speed V_p , the geomagnetic activity index Dst, the geomagnetic K_p index, and the intensity variation profiles of the ZSMT cosmic rays $N(\%)$ with an expanded time scale for the period 21–29 June 2015. The positions of the shock and the SSC are marked. The SSC time is typically related to the arrival of a shock hitting the Earth. ICME lies to the right of the SSC (the blue shaded region).

Four shocks passed through the WIND at 16:04 UT (shock1) on 21 June 2015, at 05:02 UT (shock2) and 18:08 UT (shock3) on 22 June 2015, and at 13:07 UT (shock4) on 24 June 2015, and caused a series of FDs from 21 to 30 June 2015.

Initial phase: The first shock (shock1) and second shock (shock2) passed through the WIND and caused a small increase in the V_p . Consequently, there was no significant change in the B_z . When shock2 arrived, followed by an enhanced diurnal variation, the cosmic-ray intensity variation (%) of the ZSMT did not show a significant decrease; however, the other stations showed a small decrease as shown in Fig. 5.

Pre-increase: When the third shock (shock3) was observed by WIND at 18:08 UT on 22 June 2015, Fig. 3 shows that the solar wind speed increased abruptly from 444 km/s to 672 km/s. The z-component of the IMF (B_z) suddenly dropped to -29.24 nT at 18:00 UT on 22 June 2015. The cosmic-ray intensity variation (%) of

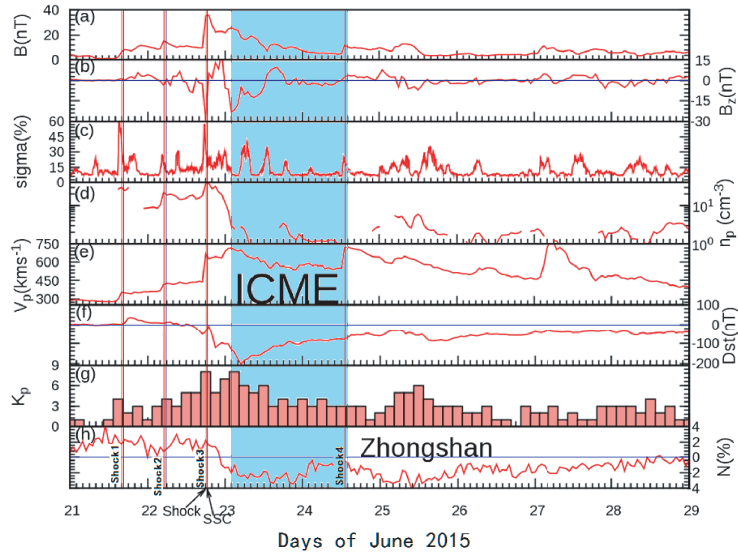


Fig. 4. (color online) Data are plotted for 21–29 June 2015. The figure from top to bottom shows the hourly values of (a) the magnetic field strength B (nT) in the GSE coordinate system, (b) the magnetic field strength B_z (nT) in the GSE coordinate system, (c) the magnetic field turbulence level σ (%)(sigma(%)), (d) the solar wind proton density n_p , (e) the solar wind proton speed V_p , (f) the geomagnetic activity index Dst, (g) K_p index, and (h) the cosmic-ray intensity variation (%) profiles of ZSMT. The times at which the shock wave passed through the WIND and SSC are shown using red and blue vertical lines, respectively. The shaded blue region indicates the interval of an ICME.

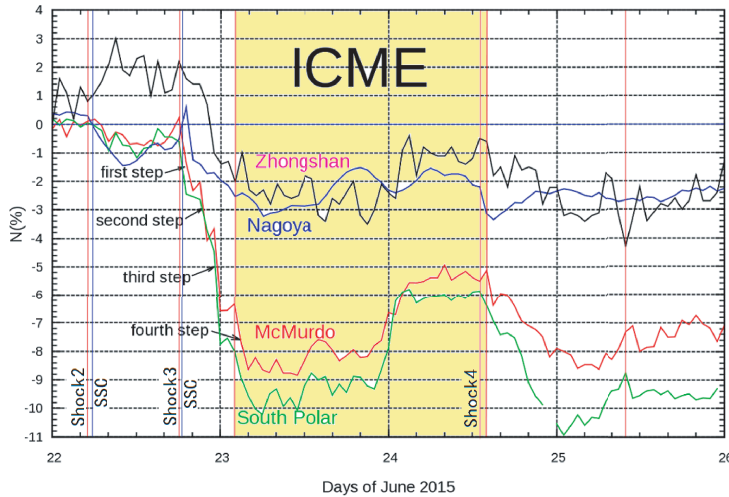


Fig. 5. (color online) Hourly cosmic-ray intensity variation (%) values of the data collected from the NM and muon telescope. The shaded yellow area indicates the interval of the ICME. Data are plotted for 22–26 June 2015. When shock 2 arrives followed by the enhanced diurnal variation, the cosmic-ray intensity variation (%) of the ZSMT shows an increasing trend whereas the other stations show a small decrease.

the ZSMT demonstrated a pre-increase ($\sim 2.3\%$) before shock3 arrived at the Earth (at 18:33 UT on 22 June 2015). Shock3 created an SSC with a geomagnetic activity index K_p of up to 8.

Main phase:The third shock (shock3) is associated with an ICME from 02:00 UT on 23 June 2015 to 14:00 UT on 24 June 2015. When the Earth entered the region between shock3 and the leading edge of the ICME,

a four-step FD occurred. The first step occurred from 19:00 UT to 20:00 UT on 23 June 2015. The hourly count decreased by approximately 0.5% that of the pre-increase. The fourth step ended at 08:00 UT on 23 June 2015 while the Earth entered the ICME. This occurred between 02:00 UT on 23 June 2015 and 14:00 UT on 24 June 2015. The cosmic-ray intensity variation (%) was approximately 2.7% relative to the mean count by the

end of the fourth step.

Recovery phase: A recovery occurred as the Earth entered a low GCR density region within the ICME. A sharp ($\sim 3\%$) recovery, shortly after the FD minimum was reached, was followed by an enhanced diurnal variation during the FD recovery phase. The complete recovery of the FD was delayed by the occurrence of shock4. The shock (shock4) was associated with an ICME from 10:00 UT on 25 June 2015 to 06:00 UT on 26 June 2015. This ICME was related to the halo CME released at 18:36 UT on 22 June 2015 and caused other counts to decrease. The counts returned to the mean value around 29 June 2015 and the recovery phase lasted until after 30 June 2015.

The southward magnetic field is the most effective interplanetary parameter for the geoeffectiveness of ICMEs. In Fig. 4, the Dst form shows a two-step process of the geomagnetic storm and a minimum of -204 nT at 05:00 UT. The first step was caused by the fluctuating southward field component of shock upstream. The second step was caused by the southward field in the ICME. Owing to the different mechanisms of geomagnetic disturbance and FDs, the Dst and FD profiles are not synchronous in Fig. 4.

The important interplanetary parameter for FDs appears to be the enhanced and turbulent magnetic field. The cosmic rays diffuse through the turbulent magnetic field in the sheath region. The turbulence level is defined as $\sigma^2 = \langle B_{\text{tur}}^2 \rangle / B_0^2$. The magnetic field B_0 is a one-hour running average of the magnetic field B . The fluctuation of the IMF around this average is $B_{\text{tur}} = B - B_0$. $\langle B_{\text{tur}}^2 \rangle$ is the average of B_{tur}^2 over the one-hour window [32]. We have calculated the turbulence level using four-minutes averaged data from the ACE/WIND spacecraft. In Fig. 4(c), the results show that the turbulence level Enhancement of close to 58% occurs at 17:36 UT on 22 June 2015. It is in the sheath region, i.e., the region between the shock and the magnetic cloud. With the scattering of cosmic-ray particles by an enhanced turbulent magnetic field in the sheath region, an FD started.

Badruddin and Anand Kumar observed that, on average, the GCR intensity during the FDs decreased at a rate of approximately 0.2% per nT change in the magnetic field during the passage of an enhanced and turbulent field region [33]. Fig. 4 shows a sharp rise in the ZSMT hourly counts (N) followed by steep variations in B_z and V_p before shock3 arrived at the Earth. This pre-

increase may result from the particles that have received a small energy boost by reflection from the approaching shock3. The main phase of decrease was caused by the ICME that accompanied shock3. When the Earth entered a region between the shock3 with the leading edge of the ICME, a three-step FD started at the arrival of shock3. This may be due to the complexities in the sheath region of turbulence. The muon flux was correlated strongly to the interplanetary condition, and it reached its minimum when the ICME enveloped the earth and the strong magnetic field prevented some of the cosmic-ray particles from reaching the Earth. Two small flux ropes in Fig. 3, FR1 and FR2, also complicate the FD process. Following the passage of shock3 and sheath structure, the Earth entered a low-GCR-density region within the ICME, and the ZSMT hourly counts returned to the mean value slowly around 30 June 2015.

The observations of GCR can be used to infer the structure of ICME even when in situ solar wind observations are not available [11]. A four-step FD started at the arrival of shock3. It may be due to complexities in the sheath region of turbulence that are not available through in situ solar wind measurements.

3.3 Galactic cosmic ray observation of the McMurdo neutron monitor, the South Pole neutron monitor, and the Nagoya muon telescope

In this work, we study the characteristics of the FD using the McMurdo and South Pole NMs data and the Nagoya muon telescope (MT) data collected in June 2015. Their properties are listed in Table 2.

The pressure-corrected hourly rates (%) from the selected NMs of the Bartol Research Institute are plotted in Fig. 5. The mean value is determined using measurements collected from 1 to 20 June 2015, before the IMF distribution. The hourly values for NMs in the Antarctic region include the South Pole and McMurdo. The values also showed occurrences of the FD formations before the shock (shock3) arrived at the Earth (SSC) at 18:33 UT on 20 June 2015. Both NMs have similar hourly-counts variations. The two NMs began to show a decrease in counting rates at 18:00 UT on 22 June 2015. The decrease occurred during the arrival of the shock (shock3) and reached the minimum at 11:00 UT on 23 June 2015 while the Earth and the ICME intersected. A sharp

Table 2. Properties of muon telescope and NMs

station	latitude (°)	longitude (°)	altitude/m	vertical cutoff rigidity/GV
Zhongshan	-69.4	76.4	11	0.07
Nagoya	35.2	137	77	11.50
South Pole	-90.0	0.0	2820	0.09
McMurdo	-77.9	166.6	48	0.00

($\sim 4\%$) recovery period, shortly after the FD minimum, was experienced. This was followed by an enhanced diurnal variation. In association with the shock (shock4) that arrived at 13:29 UT on 24 June 2015, the ICME was related to the CME released at 18:36 UT on 22 June 2015. The two NMs showed a decrease in counting rates again during this period. The McMurdo and South Pole NMs both showed a four-step decrease in count, although the decrease in count of the South Pole NM was not as evident as that of the McMurdo NM. The counts returned to their mean value, and the recovery phase ended after 30 June 2015. A slight difference was observed (while decreasing) between the counts of the McMurdo and South Pole NMs. The McMurdo NM exhibited a pre-increase in count at 18:00 UT before the shock (shock3) arrival at 18:33 UT on 22 June 2015. The South Pole NM did not exhibit a pre-increase in count.

Figure 5 shows a plot of the hourly intensity variation (%) in the vertical (V) direction for Nagoya MT. The hourly counting rate of the Nagoya MT was obtained from the GMDN data system of Shinshu University. The mean value was evaluated from the 1st to 20th day before the IMF distribution. A pre-increase was evident at 19:00 UT after the shock (shock3) arrival at the Earth (SSC) at 18:33 UT on 22 June 2015. The plot for Nagoya MT indicates that the FD onset (19:00 UT) was delayed (~ 0.5 h) with respect to the shock (shock3) arrival at the Earth (SSC). The decrease reached the minimum at 07:00 UT on 23 June 2015, while the Earth and the ICME intersected. A sharp ($\sim 2\%$) recovery period, shortly after the FD minimum was reached, was followed by enhanced diurnal variation. In association with a shock (shock4) that arrived at 13:29 UT on 24 June 2015, the hourly counts of the Nagoya MT decrease again. After the Earth intersected the ICME, which was related to the CME on 22 June 2015, the counts did not decrease in comparison with the counts of South Pole and McMurdo NMs, and the ZSMT.

The hourly cosmic ray intensity values of the South Pole and McMurdo NMs, and ZSMT have similar variations. Their hourly values when each began to decrease and reach a minimum are very similar, except that the McMurdo NM has a pre-increase and the South Pole NM does not. Nevertheless, their recovery phases are perfectly synchronized.

The FD pre-increase for Nagoya MT lags that of McMurdo and ZSMT by 1 h. The FD onset in Nagoya MT lags the onset in the South Pole, McMurdo, and ZSMT by 1 h. The cosmic-ray intensity variation scale of the ZSMT is similar to that of Nagoya MT. Our view stands that the muons collected at the two stations originate from much higher energetic particles, which receive less IMF modulation and have a similar scale of FD. Owing to the higher energy of the detection particles, the

cosmic-ray intensity variation scale of the muon telescope is less than that of the NM.

The GRAPES-3 tracking muon telescope recorded a 2-h muon burst on 22 June 2015, starting at 19:00 UT, in the midst of a continuing FD [34], which they attributed to a temporary change in the geomagnetic cut-off. Another author disagreed with this conclusion and commented on possible alternative interpretations of the GRAPES event [35]. These alternative interpretations were only used on the observation data collected from the NM. The precursor effects in different FDs have been investigated by the worldwide neutron monitor network [36]. By investigating this event using only NMs, we restrict ourselves. The muon telescope data should also be used for more in-depth investigations. However, by using the worldwide muon telescope network, we will collect additional information on the pre-increase of the FD on 22 June 2015.

3.4 ENLIL model of CME propagation

In June 2015, four halo CMEs i.e., on 18 June, 19 June, 21 June, and 22 June, were ejected and reached the Earth. These CMEs and their corresponding shocks were investigated using an application of the WSA-ENLIL model. We now focus on the CME on 21 June 2015.

Using the WSA-ENLIL model, which is a large-scale physics-based prediction model of the heliosphere, we proceeded with the investigation of the heliospheric effect of the CMEs. To determine the ambient solar wind initial conditions from the photospheric magnetograph data, the Wang–Sheeley–Arge model was adopted [37]. The model of the CME propagation used in this study is the “cone” model of the CME [38]. Fig. 6 shows two snapshots of the ENLIL model run at 18:00 UT on 22 June 2015, when the leading edge of the CME on 21 June 2015 was at 1 AU. The model results show the density and velocity of the solar wind in the ecliptic plane, where blue color represent low density and red/white/gray colors represent high densities (velocity) of the solar wind [39]. The result predicts the shocks produced by the CME on 21 June 2015, arriving at the WIND at 21:43 UT on 22 June 2015, which is approximately 4 h later than the observed shock arrival time of 18:08 UT on 22 June 2015 at the WIND. While modeling the three CMEs, each CME was treated independently. The same active region produced two other CMEs for a few days surrounding the investigation date; the model should consider changes owing to earlier CMEs, which altered the ambient background solar wind. In the model, lags in the arrival time of the ICME probably originate from the interaction between the ICME and the ambient medium, which can be disturbed by the previous two CMEs [40]. Additional ENLIL simulations of the CMEs on 18 June, 19 June, and 22 June 2015 were performed,

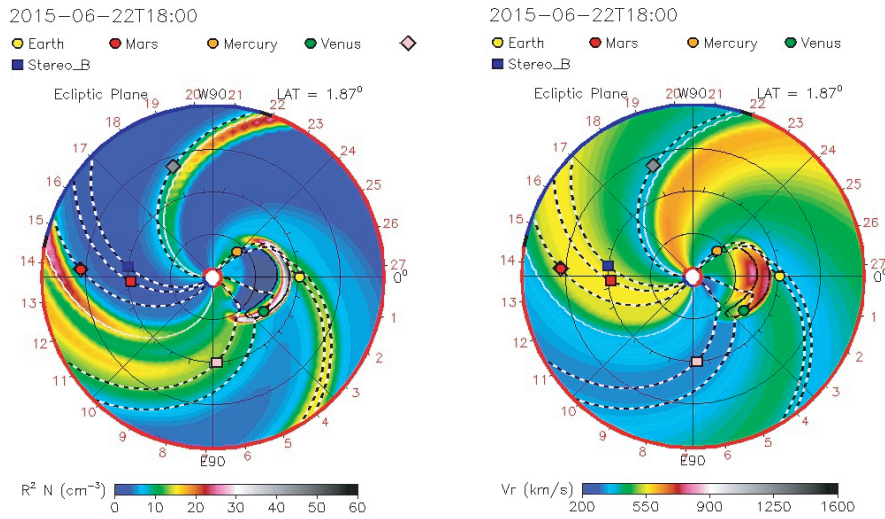


Fig. 6. (color online) Snapshots of the ENLIL model run during the propagation of the CME on 21 June 2015 through the inner heliosphere [39]. The data shown are for 18:00 UT on 22 June 2015. The figures show the density (left) and velocity (right) of the solar wind. The Sun is marked by the white circle and the Earth is indicated by the yellow circle.

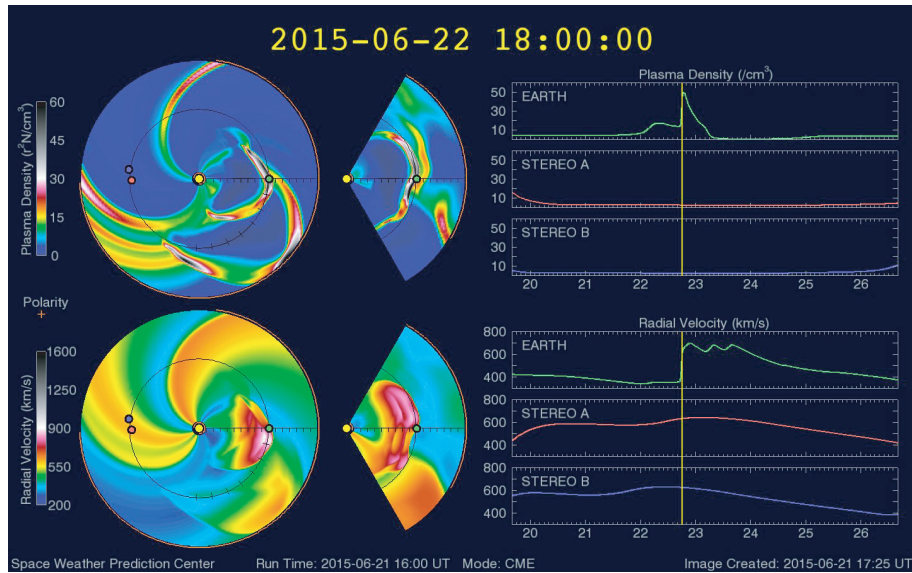


Fig. 7. (color online) Results of the ENLIL model for the CMEs on 18, 19, and 21 June 2015. The snapshots show density (top-left) and velocity (lower-left) of the solar wind at 18:00 UT on 22 June 2015. The figures show density (top-right) and velocity (lower-right) of the solar wind from 16:00 UT on 19 June 2015 to 16:00 UT on 26 June 2015. The Sun is marked by the yellow circle and the Earth is indicated by the green circle.

but they are not shown here.

The same active region produced two additional CMEs during 18–19 June, which were pushed (or compressed) along by the faster Earth-directed CME on 21 June 2015. We include the fast CME on 21 June 2015 and the previous two (slow) CMEs in a single run to investigate the interactions between CMEs [41]. The results predict the density and velocity of the solar wind in Fig. 7. This is similar to the solar wind measurements

from WIND (Fig. 3) before the propagation of the CME on 22 June 2015 through the Earth. As the CME on 22 June 2015 was not included, the results are not similar to the solar wind measurements from WIND, when the maximum solar wind speed was 724 km/s, during the period from the disturbance of the shock to the trailing edge of the ICME.

The model shows that a detector encounters regions with distinct plasma as the ICME passes the detector.

According to the traversal of the detected ICMEs near the ICME center, intermediate regions, and far away from the center, we can also estimate the amplitudes of FDs and predict their recovery characteristics [42]. According to Fig. 7, the ICME that passes the detector from the central part produces a large FD amplitude and fast recovery of the GCR intensity.

4 Summary

At Zhongshan Station in Antarctica, a cosmic-ray muon telescope (ZSMT) was installed in 2004. The pressure change at Zhongshan station was strong; thus, a pressure correction of the muon data was required to accurately analyze the ZSMT-based data. The resulting pressure-corrected counting rates show that most of the large variations in count rate are likely caused by pressure fluctuations.

From 18 to 22 June 2015, four halo CMEs headed toward the Earth. Four shocks that accompanied these CMEs passed the WIND and produced a series of FDs. We studied the characteristics of this series of FDs using data from muon telescopes (ZSMT and Nagoya MT) and NMs (South Pole and McMurdo).

According to multi-station observations, the FD that occurred on 22 June 2015 had a profile resembling a four-step decrease. The traditional FD models predict that an ICME and its shock reduce the GCR intensity and result in a two-step profile. Jordan suggested that each FD must be analyzed separately, according to its specific interplanetary circumstances [12]. In this sense, the FD of 22 June 2015 is similar to the FD of 18 February 2011 [43]. The FD of 22 June 2015 was a special four-step profile because the same active region produced two other CMEs in the earlier few days. It is likely the result of an interaction between the faster CME of 21 June and the two previous slow CMEs. The first step was caused by the shock. The second and third steps were caused by the sheath region with complex structures. The last step originated from the region of ICME.

The hourly cosmic-ray intensity values of the South Pole, McMurdo, and ZSMT have similar variations. There is a difference in the GCRs recorded between polar locations and non-polar locations. The FD pre-increases

of 22 June were collected from the Nagoya muon telescope (non-polar location) but lagged those of McMurdo and ZSMT (polar locations) by 1 h. The FD onset of 22 June for Nagoya MT lags those of the polar locations by 1 h. Owing to the higher energy of the detection particles, the cosmic-ray intensity variation scale of the muon telescope is less than that of the NM. The ZSMT cosmic-ray intensity variation scale is similar to that of the Nagoya MT.

Owing to a very small detection area, the ZSMT counting rate fluctuations were too large. We plan on extending the detection area in future work. By the end of 2015, the ZSMT was enlarged to a $1\text{ m} \times 1\text{ m}$ area consisting of eight $0.5\text{ m} \times 0.5\text{ m}$ detectors. In addition, the observational data achieved real-time transmission via satellite link, allowing a real-time data exchange between the Zhongshan station and worldwide cosmic ray observatories (e.g., NMDB (real-time database for high-resolution neutron monitor measurements) and SPACE-SHIP EARTH) that promote the joint study of the space environment.

We are grateful to Yasushi Muraki, V. Yanke, and A. Belov for their assistance. We would like to express our appreciation to the staff (Liu Yang and Shen Xin) of the Zhongshan station for their valuable work. We thank the ACE SWEPAM instrument team and the ACE Science Center for providing the ACE data. The neutron-monitor data are provided by the University of Delaware department of Physics and Astronomy and the Bartol Research Institute with support from the U.S. National Science Foundation under grant ANT-0838839. We thank the Cosmic Ray Experimental Science Team for providing the Global Muon Detector Network (GMDN) data of Shinshu University. The results presented in this paper rely on geomagnetic indices calculated and made available by ISGI Collaborating Institutes from data collected at magnetic observatories. We thank the involved national institutes, the INTERMAGNET network and ISGI (isgi.unistra.fr). We thank the Community Coordinated Modeling Center for the ENLIL model result. The authors also thank the anonymous reviewers for their detailed and constructive comments in evaluating this paper.

References

- 1 S. E. Forbush, *Physical Review*, **51**: 1108-1109 (1937)
- 2 V. F. Hess and A. Demmelmair, *Nature*, **140**: 316-317 (1937)
- 3 S. Chapman, *Nature*, **140**: 423-424 (1937)
- 4 S. B. Treiman, *Physical Review*, **89**: 130-133 (1953)
- 5 J. A. Simpson, *Physical Review*, **94**: 426-440 (1954)
- 6 C. Y. Fan, Peter Meyer, and J. A. Simpson, *Physical Review Letters*, **5**: 269-271 (1960)
- 7 O. Adriani et al, *Science*, **332**: 69-72 (2011)
- 8 T. R. Sanderson et al, 1991, Proceeding of 22nd ICRC, (Dublin 1991), pp.593-596
- 9 J. A. Lockwood, W. R. Webber, and H. Debrunner, *Journal of Geophysical Research*, **96**: 11587-11604 (1991)
- 10 G. Wibberenz et al, *Space Science Reviews*, **83**: 309-348 (1998)
- 11 H. V. Cane, *Space Science Reviews*, **93**: 55-77 (2000)
- 12 A. P. Jordan et al, *Journal of Geophysical Research*, **116**: A11103 (2011)
- 13 A. Wawrzynczak and M. V. Alania, *Advances in Space Re-*

- search, **41**: 325-334 (2008)
- 14 K. Leerunnavarat and D. Ruffolo, *The Astrophysical Journal*, **593**: 587-596 (2003)
- 15 K. Munakata et al, *Geophysical Research Letters*, **32**: L03S04 (2005)
- 16 V. Bindi, *Proceeding of 35rd ICRC (Busan, 2017)*
- 17 M. Rockenbach et al, *Space Science Reviews*, **182**: 1-18 (2014)
- 18 J. L. Zhang et al, *Nuclear Instruments and Methods in Physics Research A*, **623**: 1030-1034 (2010)
- 19 D. H. Huang et al, *Chin. J. Space Sci.*, **36**(6): 897-903 (2016) (in Chinese)
- 20 <http://yb.jnm.ihep.ac.cn/muzhongshan8>
- 21 Y. Q. Tang, H. Lu Hong et al, *Chin. J. Space Sc.*, **24**(3): 219-225 (2004) (in Chinese)
- 22 https://cdaw.gsfc.nasa.gov/CME_list/
- 23 <http://www.srl.caltech.edu/ACE/ASC/DATA/level3/icmetable2.htm>
- 24 M. Piersanti et al, *Solar Physics*, **292**: 169 (2017)
- 25 https://cdaw.gsfc.nasa.gov/CME_list/UNIVERSAL/2015.06/univ2015.06.html
- 26 https://www.cfa.harvard.edu/shocks/wi_data/
- 27 http://isgi.unistra.fr/data_download.php
- 28 L. W. Klein, L. F. Burlaga, *Journal of Geophysical Research*, **87**: 613-624 (1982)
- 29 R. P. Lepping, J. A. Jones, and L. F. Burlaga, *Journal of Geophysical Research*, **95**: 11957-11965 (1982)
- 30 M. A. Hidalgo, T. Nieves-Chinchilla, and J. J. Blanco, *Solar Physics*, **284**: 151-166 (2013)
- 31 Y. D. Liu, H. D. Hu, R. Wang et al, *The Astrophysical Journal Letters*, **809**: L34 (2015)
- 32 K. P. Arunbabu et al, *Astronomy & Astrophysics*, **580**: A41 (2015)
- 33 Badruddin, Anand Kumar, *Solar Physics*, **290**: 1271-1283 (2015)
- 34 P. K. Mohanty et al, *Proceeding of 35rd ICRC (Busan, 2017)*
- 35 The IceCube Collaboration, P. S. Mangard et al, *Proceeding of 35rd ICRC (Busan, 2017)*
- 36 M. Papailiou, H. Mavromichalaki, A. Belov, E. Eroshenko, and V. Yanke, *Solar Physics*, **276**: 337-350 (2012)
- 37 C. N. Arge, V. J. Pizzo, *Journal of Geophysical Research*, **105**: 10465-10497 (2000)
- 38 H. Xie, L. Ofman, G. Lawrence, *Journal of Geophysical Research*, **109**: A03109 (2004)
- 39 <https://kauai.ccmc.gsfc.nasa.gov/CMEscoreboard/>
- 40 Y. D. Liu et al, *The Astrophysical Journal*, **769**: 45 (2013)
- 41 <https://www.ngdc.noaa.gov/enlil/>
- 42 A. Kumar, Badruddin and M. Derouich, *Solar Physics*, **292**: 166 (2017)
- 43 A. Papaioannou et al, *Journal of Physics: Conference Series*, **409**: 012202 (2013)